

# Non-equilibrium transport theory of the singlet-triplet transition: perturbative approach

B. Horváth<sup>1</sup>, B. Lazarovits<sup>1,2</sup>, and G. Zaránd<sup>1</sup>

<sup>1</sup>*Theoretical Physics Department, Institute of Physics,*

*Budapest University of Technology and Economics, Budafoki út 8, H-1521 Hungary*

<sup>2</sup>*Research Institute for Solid State Physics and Optics of the Hungarian Academy of Sciences, Konkoly-Thege M. út 29-33., H-1121 Budapest, Hungary*

We use a simple iterative perturbation theory to study the singlet-triplet (ST) transition in lateral and vertical quantum dots, modeled by the non-equilibrium two-level Anderson model. To a great surprise, the region of stable perturbation theory extends to relatively strong interactions, and this simple approach is able to reproduce all experimentally-observed features of the ST transition, including the formation of a dip in the differential conductance of a lateral dot indicative of the two-stage Kondo effect, or the maximum in the linear conductance around the transition point. Choosing the right starting point to the perturbation theory is, however, crucial to obtain reliable and meaningful results.

PACS numbers: 73.63.Kv, 73.23.-b, 72.10.Fk

## I. INTRODUCTION

With the evolution of mesoscopic and nano-scale technology and electron lithography, physicists gain more and more control over sub-micron structures and molecular devices.<sup>1-4</sup> By exploiting cutting-edge semiconductor technology, experimentalists can now not only build artificial atoms and molecules to trap and manipulate individual electrons and their spin,<sup>5,6</sup> but they are also able to contact and gate real molecules,<sup>7</sup> and build simple molecular devices out of them such as the single electron transistor. These devices are promising candidates for our future electronics, and might possibly be used as building blocks of spintronics devices and spin-based quantum computers, too.<sup>8</sup> Moreover, the unprecedented control of these minuscule structures opens new and fascinating possibilities to build and study hybrid structures,<sup>9-13</sup> entangle electron spins,<sup>14</sup> and also to realize and study simple quantum systems in the close vicinity of quantum phase transitions under non-equilibrium conditions.<sup>15-19</sup>

Understanding the physical properties of these tiny electronic circuits represents a major challenge to theoretical as well as to experimental physicists. Due to their extremely small size, electron-electron interaction is often dominant in these structures, and moreover, as mentioned before, they are operated under non-equilibrium conditions. Although theoretical physicists devoted a lot of effort to design methods that are able to tackle these difficulties, so far none of the proposed methods proved to be entirely successful in describing strongly interacting non-equilibrium systems: Monte Carlo methods are presently unable to reach the required precision,<sup>20,21</sup> Bethe Ansatz methods can be used for a few models only, and are still in an experimental stage,<sup>22-24</sup> and perturbative renormalization group methods can only reach a particular region of the parameter space.<sup>25-28</sup> Maybe numerical renormalization group methods are currently the most reliable techniques to study these non-equilibrium

systems,<sup>24,29,30</sup> however, they scale very badly with the number of states involved, and to compute the transport through just two levels in the presence of interaction seems to be numerically too demanding.

In view of the above-described situation, perturbative methods such as iterative perturbation theory (IPT),<sup>31-33</sup> e.g., are of great value, especially, since many well-contacted or almost open systems are *de facto* in the perturbative regime. For this reason, several molecular electronics groups combine the GW method with standard *ab initio* tools to compute transport through molecules.<sup>34</sup> Unfortunately, however, very little is known about the reliability of this approach. It is, e.g., rather easy to obtain spontaneous local symmetry breaking (e.g., magnetic moment formation), and thereby obtain physically incorrect results.<sup>35</sup>

In the present paper we investigate systematically the perturbative approach for the simplest possible non-trivial molecular system, a two-level Anderson model with two degenerate or nearly degenerate electron levels. This simple model describes many experimental systems, and it displays rich physical properties. Having an odd number of electrons on the two levels, e.g., one can recover an almost SU(4) symmetrical Kondo state.<sup>36-40</sup> In case of two electrons, on the other hand, one finds a transition (cross-over) between a state, where the two electrons are bound into a *singlet*, and another state, where the two electrons' spin is aligned into a *triplet*, which is then completely or partially screened by the spin of the conduction electrons in the leads.<sup>16,17,41-44</sup> Here we focus our attention to this second, most interesting regime, also nicknamed as the singlet-triplet (ST) transition. We focus on the most realistic case,<sup>43</sup> where two independent conduction electron channels are coupled to the dot levels, and therefore the singlet-triplet transition is just a cross-over.<sup>41-44</sup> This must be contrasted to the case of a single coupled conduction electron channel, when the transition is a true Kosterlitz-Thouless quantum phase transition.<sup>16,17</sup> Non-equilibrium transport in this latter

case has been investigated recently using the so-called non-crossing approximation (NCA).<sup>45</sup>

Describing the case of two coupled channels under non-equilibrium conditions represents a theoretical challenge. The deep singlet side of the transition is accessible through perturbative renormalization group methods, which were used successfully to analyze the non-equilibrium transport in this perturbative regime.<sup>46</sup> Here we focus on the transition, and investigate, whether a simple perturbative approach is able to account for the transition between the two correlated states. To our surprise, perturbation theory captures all qualitative features of the transition, including the two-stage Kondo effect, or the conductance maximum around the transition point.<sup>41–44</sup> However, to obtain accurate perturbative results, one needs to expand around the best possible non-interacting theory.<sup>31–33</sup> This we achieve by introducing self-consistently determined counterterms, which is essentially equivalent to doing perturbation theory around the Hartree solution.

The simple perturbative calculation is, however, unable to capture correctly the Kondo scales, i.e. the energy scales below which the electron spins on the dot are screened or bound to a singlet. As we show in a Ref. 47, this shortcoming of the iterative perturbation theory can be overcome to a large extent by the so-called Fluctuation Exchange Approximation (FLEX) extended to non-equilibrium situations.

The paper is organized as follows. In Secs. II A and II B, we introduce the non-equilibrium two-level Anderson model, and describe the iterative perturbation theory used to solve the non-equilibrium Anderson model. In Sec. II C we show how to obtain the transport properties. Some computational details and the limitations of the iterative perturbation scheme are given in sections II D and II E. In Sec. III A, we discuss the results obtained for completely symmetrical quantum dots with equal level widths, while in Sec. III B results for dots with more generic parameters are presented. Our conclusions are summarized conclude in Sec. IV, and some technical details are given in Appendix A.

## II. THEORETICAL FRAMEWORK

### A. Model

The physical properties of a quantum dot with even number of electrons are usually well-captured by a simple two-level Anderson Hamiltonian. This can be written as a sum of a non-interacting and an interacting term:  $H = H_0 + H_{\text{int}}$ . The non-interacting part,  $H_0$ , can be further divided into three terms,

$$H_0 = H_{\text{cond}} + H_{\text{hyb}} + H_{0,\text{dot}}. \quad (1)$$

Here  $H_{\text{cond}}$  describes conduction electrons in the leads,  $H_{\text{hyb}}$  accounts for the hybridization between the conduction electrons and the electrons residing on the dot,

and  $H_{0,\text{dot}}$  stands for the non-interacting part of the dot Hamiltonian,

$$H_{0,\text{dot}} = \sum_{i,\sigma} \varepsilon_i d_{i\sigma}^\dagger d_{i\sigma}, \quad (2)$$

with  $d_{i\sigma}^\dagger$  the creation operator of a dot electron of spin  $\sigma$  on dot level  $i$  of energy  $\varepsilon_i$  ( $i \in (+, -)$ ).

The precise form of  $H_{\text{cond}}$  and  $H_{\text{hyb}}$  depends on the geometrical arrangement of the quantum dot. In case of a lateral quantum dot close to pinch-off, there is only a single conduction electron mode coupled to the dot, and correspondingly,

$$H_{\text{cond}}^{\text{lat}} = \sum_{\xi,\alpha,\sigma} \xi_\alpha c_{\xi\alpha\sigma}^\dagger c_{\xi\alpha\sigma}, \quad (3)$$

$$H_{\text{hyb}}^{\text{lat}} = \sum_{\alpha,i,\xi,\sigma} t_{\alpha i} (c_{\xi\alpha\sigma}^\dagger d_{i\sigma} + h.c.). \quad (4)$$

Here  $c_{\xi\alpha\sigma}^\dagger$  creates a conduction electron in the left or right lead ( $\alpha \in (L, R)$ ) with energy  $\xi_\alpha = \xi + \mu_\alpha$ , with  $\mu_\alpha = eV_\alpha$  the bias applied on lead  $\alpha$ . The  $t_{\alpha i}$ 's denote tunneling matrix elements between lead  $\alpha$  and dot level  $i$ , and for the sake of simplicity here we assume them to be spin- and energy independent.

Vertical quantum dots<sup>48–50</sup> or nanotubes<sup>51</sup> are, on the other hand, often connected to leads with a large surface and therefore in each lead there are typically many different conduction electron modes which couple to a given dot state. However, for each dot state  $i$  and lead  $\alpha$ , one can construct a single linear combination of modes,  $d_{i\sigma}^\dagger \rightarrow c_{\xi,i\alpha\sigma}^\dagger$ , which hybridizes with  $d_{i\sigma}$ . In many cases, one can assume (based on symmetry considerations or in view of the chaotic shape of the dot wave functions and the large number of lead modes) that  $c_{\xi,i\alpha\sigma}^\dagger$  are independent of each other for  $i = \pm$  i.e.  $\{c_{\xi,+,\alpha,\sigma}^\dagger, c_{\xi,-,\alpha,\sigma}\} = 0$ . Under this assumption,  $H_{\text{cond}}$  and  $H_{\text{hyb}}$  assume the form,

$$H_{\text{cond}}^{\text{vert}} = \sum_{\xi,i,\alpha,\sigma} \xi_\alpha c_{\xi i\alpha\sigma}^\dagger c_{\xi i\alpha\sigma}, \quad (5)$$

$$H_{\text{hyb}}^{\text{vert}} = \sum_{\alpha,i,\xi,\sigma} t_{\alpha i} (c_{\xi i\alpha\sigma}^\dagger d_{i\sigma} + h.c.). \quad (6)$$

Notice that the non-equilibrium condition is taken into account through a lead-dependent shift of the chemical potentials, and the interaction between the conduction electrons is neglected.

In general, the hybridization matrix elements  $t_{\alpha i}$  are independent of each-other. However, for simplicity, in this paper we focus on completely *symmetrical* quantum dots and assume further that one of the dot levels is even (+), while the other is odd under reflection (−). As a consequence, for a lateral dot the tunneling matrix elements have a simple structure:  $t_{L,+} = t_{R,+}$  and  $t_{L,-} = -t_{R,-}$ . Although this choice may seem to be too special, this symmetrical model still captures most of the generic features of a two-level quantum dot.<sup>43,44</sup>

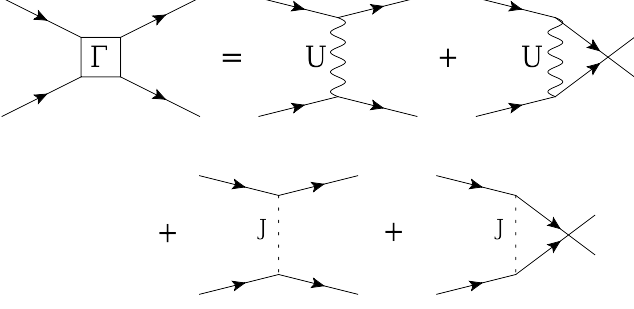


FIG. 1: The antisymmetrized vertex function containing the Coulomb interaction and the Hund's rule coupling.

In our model, electron-electron interaction on the dot is taken into account by the term:

$$H_{\text{int}} = \frac{U}{2} \left( \sum_{i,\sigma} n_{i\sigma} - 2 \right)^2 - J \vec{S}^2, \quad (7)$$

where  $n_{i\sigma} = d_{i\sigma}^\dagger d_{i\sigma}$  and  $\vec{S} = \frac{1}{2} \sum_{i,\sigma,\sigma'} d_{i\sigma}^\dagger \vec{\sigma}_{\sigma\sigma'} d_{i\sigma'}$  with  $\vec{\sigma}$  denoting the Pauli matrices,  $\vec{\sigma} = (\sigma_x, \sigma_y, \sigma_z)$ . Here the coupling constant  $U$  denotes the on-site Coulomb interaction, and accounts for the charging energy of the dot, while  $J$  stands for the Hund's rule coupling, favoring a ferromagnetic alignment of the dot electron spins ( $J > 0$ ). In this work, we focus our attention to the regime where approximately two electrons reside on the dot. This assumption is implicit in the way we expressed the Coulomb term in Eq. (7), which obviously possesses a particle-hole symmetry discussed later.

Although Eq. (7) provides a rather symmetrical and compact expression for the interaction term, for the purpose of a systematic perturbation theory, it is useful to rewrite it in a normal ordered form,

$$H_{\text{int}} = : H_{\text{int}} : - \left( \frac{3U}{2} + \frac{3J}{4} \right) \sum_{i,\sigma} n_{i\sigma}, \quad (8)$$

and treat only the normal ordered part as a perturbation,  $: H_{\text{int}} :$ , while adding the second term in this expression to  $H_{0,\text{dot}}$ ,

$$\epsilon_i \rightarrow E_i \equiv \epsilon_i - \frac{3J}{4} - \frac{3U}{2}. \quad (9)$$

We remark that for a two-level dot close to half filling,  $\epsilon_i \approx 0$ , and the point  $\epsilon_+ = \epsilon_- = 0$  corresponds to the case where the two levels are exactly degenerate, and there are exactly two electrons on the dot ( $\langle \sum_{i\sigma} n_{i\sigma} \rangle = 2$ ).

For later purposes, let us give here the explicit form of  $: H_{\text{int}} :$  as obtained by exploiting fermionic commutation

relations,

$$\begin{aligned} : H_{\text{int}} : = & -\frac{J}{2} \sum_{\sigma} \sum_{i \neq j} d_{i\sigma}^\dagger d_{j\bar{\sigma}}^\dagger d_{j\sigma} d_{i\bar{\sigma}} + \\ & + \left( \frac{U}{2} + \frac{3J}{4} \right) \sum_{i,\sigma} d_{i\sigma}^\dagger d_{i\bar{\sigma}}^\dagger d_{i\bar{\sigma}} d_{i\sigma} + \\ & + \left( \frac{U}{2} - \frac{J}{4} \right) \sum_{i \neq j, \sigma} d_{i\sigma}^\dagger d_{j\bar{\sigma}}^\dagger d_{j\sigma} d_{i\sigma} + \\ & + \left( \frac{U}{2} + \frac{J}{4} \right) \sum_{i \neq j, \sigma} d_{i\sigma}^\dagger d_{j\bar{\sigma}}^\dagger d_{j\bar{\sigma}} d_{i\sigma}, \quad (10) \end{aligned}$$

where  $\bar{\sigma} = -\sigma$ . To simplify perturbation theory, it is useful to collect all fourth order terms and rewrite  $: H_{\text{int}} :$  in terms of the antisymmetrized interaction vertex shown in Fig. 1,  $\Gamma_{i\sigma n\bar{\sigma}}^{j\sigma' m\bar{\sigma}'}$ , as

$$: H_{\text{int}} := \sum_{\substack{i,j,m,n \\ \sigma,\sigma',\bar{\sigma},\bar{\sigma}'}} \frac{1}{4} \Gamma_{i\sigma n\bar{\sigma}}^{j\sigma' m\bar{\sigma}'} d_{j\sigma'}^\dagger d_{m\bar{\sigma}'}^\dagger d_{n\bar{\sigma}} d_{i\sigma}. \quad (11)$$

Using the fact that  $\Gamma_{i\sigma n\bar{\sigma}}^{j\sigma' m\bar{\sigma}'}$  is anti-symmetrical under exchanging  $i\sigma \leftrightarrow n\bar{\sigma}$  and  $j\sigma' \leftrightarrow m\bar{\sigma}'$ , it is easy to read out the non-vanishing matrix elements of  $\Gamma_{i\sigma n\bar{\sigma}}^{j\sigma' m\bar{\sigma}'}$  from Eq. (10). Although the vertex  $\Gamma$  has formally 256 elements, as a consequence of spin and level-conservation in Eq. (10), only thirty-two of these enter actual calculations. The advantage of the symmetrical form, Eq. (11), is that it allows one to treat the Coulomb interaction and the Hund's rule coupling on equal footing: one can formally (and numerically) evaluate the self energy diagrams shown schematically in Fig. 2, with the specific form of the interaction hidden in the internal structure of these diagrams showing in Fig. 1.

Before proceeding with the presentation of our non-equilibrium perturbation theory, let us shortly discuss the symmetry properties of the Hamiltonian. Clearly,

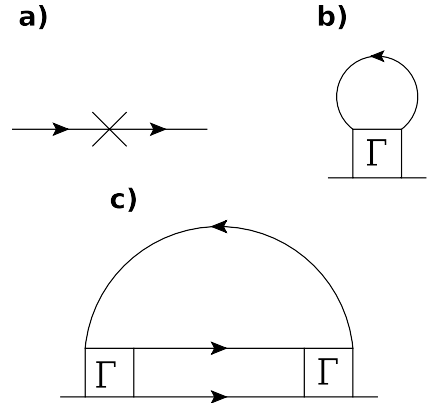


FIG. 2: Counterterm (a), first order (b) and second order (c) contributions to the self-energy. The lines denote non-interacting Keldysh Green's functions.

$H$  is invariant under  $SU(2)$  *spin rotations*. This implies that, in the absence of an external magnetic field, all Green's functions are diagonal in the spin labels and also independent of them.

In addition to spin  $SU(2)$  symmetry, depending on the specific Hamiltonian parameters,  $H$  may also possess a discrete *electron-hole* symmetry. In fact, throughout the present paper we shall restrict ourself to the simple case, where the two levels  $\epsilon_{\pm}$  are shifted symmetrically away from 0,

$$\epsilon_{\pm} = \pm \Delta/2. \quad (12)$$

Then, for  $|t_{\alpha+}| = |t_{\alpha-}|$ , the Hamiltonian is also invariant under the following transformation:

$$\begin{aligned} (d_{+, \uparrow}^{\dagger}, d_{+, \downarrow}^{\dagger}) &\leftrightarrow (d_{-, \downarrow}, -d_{-, \uparrow}), \\ (c_{\xi, L \uparrow}^{\dagger}, c_{\xi, L \downarrow}^{\dagger}) &\leftrightarrow (-c_{-\xi, R \downarrow}, c_{-\xi, R \uparrow}). \end{aligned} \quad (13)$$

This symmetry implies that the occupation of the dot is exactly  $\langle \sum_{i, \sigma} n_{i\sigma} \rangle \equiv 2$  for any interaction strength and splitting  $\Delta$ , and also implies the relation

$$\varrho_+(\omega) = \varrho_-(-\omega),$$

between the spectral functions  $\varrho_{\pm}$  of the two dot levels. [For a precise definition, see Eq. (33)]

Finally, at the special point,  $\epsilon_+ = \epsilon_- = 0$ , we have yet another electron-hole symmetry, satisfied even for  $|t_{\alpha+}| \neq |t_{\alpha-}|$ ,

$$\begin{aligned} (d_{\alpha, \uparrow}^{\dagger}, d_{\alpha, \downarrow}^{\dagger}) &\leftrightarrow (d_{\alpha, \downarrow}, -d_{\alpha, \uparrow}), \\ (c_{\xi, L \uparrow}^{\dagger}, c_{\xi, L \downarrow}^{\dagger}) &\leftrightarrow (-c_{-\xi, R \downarrow}, c_{-\xi, R \uparrow}). \end{aligned} \quad (14)$$

This second symmetry implies the spectral function relations,  $\varrho_+(\omega) = \varrho_+(-\omega)$  and  $\varrho_-(\omega) = \varrho_-(-\omega)$ .

## B. Out of equilibrium iterative perturbation theory

To describe the transport properties of a quantum dot under out of equilibrium conditions, we shall apply the so-called Keldysh Green function technique.<sup>52</sup> However, before doing so, let us further reorganize our Hamiltonian. Clearly, interactions can substantially shift the effective values of the dot energies. Therefore, to account for this trivial but possibly large renormalization effect, we apply a counterterm procedure: We take as a non-interacting part the following Hamiltonian

$$\tilde{H}_0 \equiv H_{\text{cond}} + H_{\text{hyb}} + \sum_{i, \sigma} \tilde{\epsilon}_{i\sigma} d_{i\sigma}^{\dagger} d_{i\sigma}, \quad (15)$$

while the rest of the Hamiltonian is treated as a perturbation,

$$\tilde{H}_{\text{int}} \equiv : H_{\text{int}} : + H_{\text{count}}, \quad (16)$$

$$H_{\text{count}} \equiv \sum_{i, \sigma} (E_i - \tilde{\epsilon}_{i\sigma}) d_{i\sigma}^{\dagger} d_{i\sigma}. \quad (17)$$

In other words, we expand around fictitious (effective) dot levels,  $\tilde{\epsilon}_{i\sigma}$ , at the price of treating the counterterm  $H_{\text{count}}$  also as a perturbation. This approach is essentially the same as performing perturbation theory around the Hartree theory, and allows us to extend the range of validity of our perturbation theory by making a proper choice of  $\tilde{\epsilon}_{i\sigma}$  (see below).

Our primary goal is to compute the non-equilibrium Keldysh Green's functions,  $G^{\kappa, \kappa'}$ , with the index pair  $(\kappa, \kappa')$  corresponding to the branches of the Keldysh contour. With this notation  $G^{1,1}$  stands for time-ordered ( $G^T$ ),  $G^{1,2}$  for lesser ( $G^<$ ),  $G^{2,1}$  for larger ( $G^>$ ), and  $G^{2,2}$  for the anti-time-ordered ( $G^{\bar{T}}$ ) Green's functions. These are related to the usual retarded ( $R$ ), advanced ( $A$ ) and Keldysh ( $K$ ) Green's functions by the usual relations<sup>52</sup>

$$G^R = G^T - G^<, \quad (18)$$

$$G^A = G^T - G^>, \quad (19)$$

$$G^K = G^T + G^{\bar{T}}, \quad (20)$$

and also satisfy the restriction,  $G^T + G^{\bar{T}} = G^< + G^>$ .

To determine the interacting dot Green's functions,  $G_{i\sigma, i'\sigma'}^{\kappa\kappa'}$ , we perform perturbation theory in  $\tilde{H}_{\text{int}}$  by taking  $\tilde{H}_0$  as a non-interacting Hamiltonian. The Green's function can thus be expressed in terms of the self-energy  $\Sigma_{i\sigma, i'\sigma'}^{\kappa\kappa'}$  and the unperturbed Green's functions,  $g_{i\sigma, i'\sigma'}^{\kappa\kappa'}$  by the Dyson equation,

$$\mathbf{G}(\omega)^{-1} = \mathbf{g}(\omega)^{-1} - \Sigma(\omega). \quad (21)$$

where a matrix notation  $A_{i\sigma, i'\sigma'}^{\kappa\kappa'} \rightarrow \mathbf{A}$  has been introduced. The non-interacting Green's functions corresponding to the resonant level model  $\tilde{H}_0$  can be easily computed, and are listed in Appendix A. Up to second order in the interaction, the self-energy can formally be written as

$$\Sigma(\omega) = \Sigma^{(\text{count})} + \Sigma^{(1)} + \Sigma^{(2)}(\omega) + \dots, \quad (22)$$

where the different terms denote the counterterm, the first and second order terms shown in Fig. 2. An explicit evaluation of the diagrams in Fig. 2 gives the following results:

$$\Sigma^{(\text{count})}_{ii'\sigma}{}^{\kappa\kappa'} = \delta_{\kappa\kappa'} \delta_{ii'} s_{\kappa} (E_i - \tilde{\epsilon}_{i\sigma}),$$

$$\Sigma^{(1)}_{ii'\sigma}{}^{\kappa\kappa'} = \delta_{\kappa\kappa'} s_{\kappa} \int_{-\infty}^{\infty} \frac{d\omega_1}{2\pi} \sum_{jj'\sigma'} \Gamma_{i\sigma j\sigma'}^{i'\sigma j'\sigma'} g_{jj'\sigma'}^{<}(\omega_1)$$

$$\Sigma^{(2)}_{ii'\sigma}{}^{\kappa\kappa'}(\omega) =$$

$$\begin{aligned} &= s_{\kappa} s_{\kappa'} \sum_{\substack{j, m, n \\ j', m', n' \\ \sigma', \sigma'', \sigma'''}} \Gamma_{i\sigma n\sigma'''}^{j\sigma' m\sigma''} \Gamma_{j'\sigma' n\sigma'''}^{i'\sigma n'\sigma'''} \int_{-\infty}^{\infty} \frac{d\omega_1}{2\pi} \int_{-\infty}^{\infty} \frac{d\omega_2}{2\pi} \times \\ &\times g_{jj'\sigma'}^{\kappa\kappa'}(\omega_1) g_{mm'\sigma''}^{\kappa\kappa'}(\omega_2) g_{nn'\sigma'''}^{\kappa\kappa'}(\omega_1 - \omega_2 - \omega), \end{aligned} \quad (23)$$

where the Keldysh sign  $s_{\kappa}$  has been introduced to account for the sign change of the interaction term on the

Keldysh contour:  $s_1 = 1$ ,  $s_2 = -1$ . In these expressions we assumed that the  $z$ -component of the spin is conserved, and correspondingly, the Green's functions and the self-energies are diagonal in  $\sigma$ .

In principle, Eqs. (21), (22), and (23) give a complete perturbative description of the quantum dot. However, they depend parametrically on the so far unspecified levels,  $\tilde{\varepsilon}_{\pm\sigma}$ . Following the concept of iterative perturbation theory, we determine these quantities selfconsistently from Eqs. (22) and (21) by requiring that  $\mathbf{g}$  and  $\mathbf{G}$  give the same occupation numbers,<sup>31</sup>

$$\begin{aligned} n_{i\sigma}^{(0)}[\tilde{\varepsilon}_{i\sigma}] &\equiv n_{i\sigma}^{(2)}[\tilde{\varepsilon}_{i\sigma}], \\ n_{i\sigma}^{(0)}[\tilde{\varepsilon}_{i\sigma}] &= \frac{1}{2\pi i} \int_{-\infty}^{\infty} g_{ii\sigma}^<(\omega) d\omega, \\ n_{i\sigma}^{(2)}[\tilde{\varepsilon}_{i\sigma}] &= \frac{1}{2\pi i} \int_{-\infty}^{\infty} G_{ii\sigma}^<(\omega) d\omega. \end{aligned} \quad (24)$$

Condition (24) can be fulfilled by tuning the effective levels. In spite of the simplicity of this “iterative perturbation theory”, the results obtained with it show remarkable agreement with the ones obtained with more advanced techniques for several equilibrium systems.<sup>26</sup> Unfortunately, a well established and exact non-equilibrium impurity solver being not available yet, one can only judge the validity of this perturbative approach by possibly comparing with results obtained by some reliable equilibrium methods, and by investigating the internal consistency of its. As discussed in Section II E, the range of applicability turns out to be limited to small to moderate values of  $U$  and  $J$ .

In principle, Eq. (24) could and should be solved for finite biases. However, under non-equilibrium conditions, the off-diagonal elements  $\langle d_{1\sigma}^\dagger d_{2\sigma} \rangle$  become also finite, and additional constraints related to current conservation may also emerge. In this work, we rather use a different and simple strategy: we determine  $\tilde{\varepsilon}_i$  in equilibrium, and then fix it also for the non-equilibrium calculations. For not very large bias voltages this leads to a stable solution of the self-consistency equations.

### C. Transport properties

Having the Green's functions  $\mathbf{G}$  at hand, we can calculate transport properties such as current and conductance based upon the Meir–Wingreen formula<sup>53</sup>,

$$\begin{aligned} I &= \frac{ie}{2h} \sum_{\sigma} \int_{-\infty}^{\infty} d\omega \text{Tr} \left[ (\mathbf{\Gamma}^L - \mathbf{\Gamma}^R) \mathbf{G}_{\sigma}^<(\omega) + \right. \\ &\quad \left. + (f_L(\omega) \mathbf{\Gamma}^L - f_R(\omega) \mathbf{\Gamma}^R) (\mathbf{G}_{\sigma}^R(\omega) - \mathbf{G}_{\sigma}^A(\omega)) \right]. \end{aligned} \quad (25)$$

Here  $f_{\alpha}(\omega) = f(\omega - \mu_{\alpha})$  is the Fermi function in lead  $\alpha$ , and the Green's functions are matrices in the level indices

only. The difference between the formulas for lateral and vertical dots appears only in the different structure of the  $\mathbf{\Gamma}$ -matrices defined as

$$(\Gamma_{ij}^{\alpha})_{\text{lat}} = 2\pi N_0 t_{\alpha i} t_{\alpha j}^*, \quad (26)$$

in the lateral case and

$$(\Gamma_{ij}^{\alpha})_{\text{vert}} = \delta_{ij} 2\pi N_0 t_{\alpha i} t_{\alpha j}^*, \quad (27)$$

for a vertical quantum dot. These are related to the width  $\Gamma_{\pm}$  of levels  $i = \pm$  through

$$\Gamma_i \equiv \sum_{\alpha} \Gamma_{ii}^{\alpha}.$$

In our case, the ground state of the system is a Fermi liquid<sup>54</sup>. Therefore, according to Nozières's Fermi liquid theory, at  $T = 0$  temperature (and  $V = 0$  bias), quasiparticles at the Fermi energy scatter elastically from the impurity, and their scattering process can be described in terms of simple phase shifts. Since our model is invariant under reflection for  $V = 0$ , and since one of the levels is assumed to be even while the other one odd, we can characterize the scattering process at the Fermi energy by just two phase shifts,  $\delta_i$ , associated with the two dot levels. These phase shifts are related to the retarded equilibrium Green's function through the Fermi liquid relation,<sup>54</sup>

$$\delta_i = \frac{\pi}{2} - \arctan \left( \frac{\text{Im} G_{ii\sigma}^R(\omega = 0, V = 0)}{\text{Re} G_{ii\sigma}^R(\omega = 0, V = 0)} \right). \quad (28)$$

In the limit of infinite bandwidth, the phase shifts are also related to the occupation of the levels  $d_{i\sigma}$  by the Friedel sum rule,<sup>54</sup>

$$2 \frac{\delta_i}{\pi} = \langle n_i \rangle. \quad (29)$$

where  $\langle n_i \rangle = \sum_{\sigma} \langle n_{i\sigma} \rangle$ . However, for a finite conduction band cut-off Eq. (29) is only approximate, and Eq. (28) gives a more reliable way to determine the phase shift.

The  $T = 0$  linear conductance is directly related to the phase shifts above through the Landauer–Büttiker formula. For a lateral dot, an elementary calculation gives<sup>43</sup>

$$G_{\text{lin}}^{\text{lat}} = \frac{2e^2}{h} \sin^2(\delta_+ - \delta_-), \quad (30)$$

while for a vertical dot one obtains<sup>48</sup>

$$G_{\text{lin}}^{\text{ver}} = \frac{2e^2}{h} (\sin^2 \delta_+ + \sin^2 \delta_-). \quad (31)$$

These equations are very instructive, and help us to understand the transport properties of the dots. They imply, *e.g.*, that at complete resonance,  $\delta_+ = \delta_- = \pi/2$ , the conductance of a vertical dot is  $4e^2/h$ , while that of a lateral dot vanishes due to the interference of scattering



states. These interference effects are expected to show up also in the non-equilibrium results.

The equations above are also useful to test our numerical calculations. The linear conductance values in Eq. (30) and in Eq. (31) can be compared to the equilibrium limits of the differential conductances obtained by a numerical differentiation of the current as a function of the bias voltage  $dI/dV|_{V=0}$ , as computed from the Meir-Wingreen formula.

#### D. Computational details

In the numerical calculations we represented the Green's functions using a finite uniform mesh of  $N$  frequency points in the range  $-\Omega/2 < \omega < \Omega/2$ . Depending on the accuracy needed, we used slightly different values for  $\Omega$  and  $N$ . To study the range of applicability of our method, we used  $N = 2^{15}$  points and  $\Omega = 500U$ . To compute the spectral functions, we used  $N = 2^{17}$  and  $\Omega = 1000U$ , while for the current and differential conductance plots we chose  $N = 2^{17}$  and  $\Omega = 200U$ . All results presented in this paper were obtained at  $T = 0$  temperature.

The advantage of the iterative perturbation theory is that the calculation of the second order self-energy is only seemingly cumbersome. Rewriting Eq. (23) in time domain, one obtains a simple multiplication of the various components of the Green's functions,

$$\begin{aligned} \Sigma_{ii'\sigma}^{(2)\kappa\kappa'}(t) = & s_{\kappa}s_{\kappa'} \sum_{j,j',m,m',n,n',\sigma',\sigma'',\sigma'''} \Gamma_{i\sigma n\sigma'''}^{j\sigma' m\sigma''} \Gamma_{j'\sigma' m\sigma''}^{i'\sigma n'\sigma'''} \times \\ & \times g_{jj'\sigma'}^{\kappa\kappa'}(t) g_{mm'\sigma''}^{\kappa\kappa'}(t) g_{n'n\sigma'''}^{\kappa'\kappa}(-t). \end{aligned} \quad (32)$$

Thus the self-energy can be computed by just performing a Fast Fourier Transformation to get  $\mathbf{g}(t)$ , evaluating  $\Sigma(t)$  in the time domain, and then transforming it back to frequency space.

As already mentioned before, for any given set of parameters we first carried out a calculation in the absence of voltage,  $V = 0$ , and determined the levels,  $\tilde{\epsilon}_{\pm}$ . Then we computed  $\Sigma(\omega)$  and  $\mathbf{G}(t)$  using Eq. (32), computed the spectral functions

$$\varrho_{i\sigma}(\omega) = -\frac{1}{\pi} \text{Im} G_{ii\sigma}^R(\omega), \quad (33)$$

as well as the total spectral function,  $\varrho_T(\omega) = \sum_{i,\sigma} \varrho_{i\sigma}(\omega)$ , and finally evaluated the current using the Meir-Wingreen formula, Eq. (25). The differential conductance has been obtained by direct numerical differentiation of the current,  $G(V) = dI(V)/dV$ .

#### E. Limitations

Perturbation theory has a limited range of validity. For large values of the interaction,  $U$ , a spontaneous symmetry breaking occurs, whereby the occupation of the dot

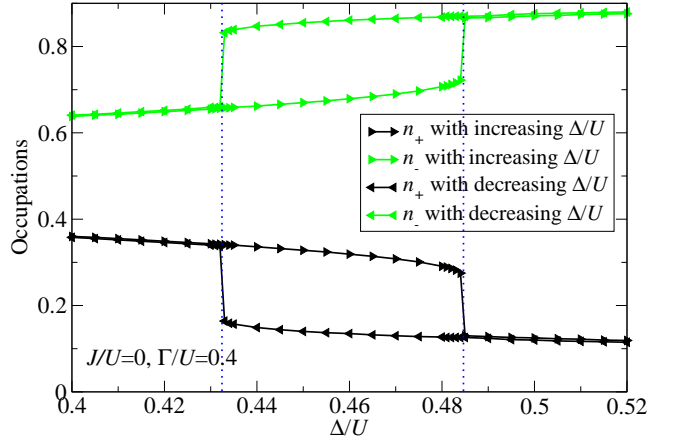


FIG. 3: (Color online) Hysteresis of the occupation number as a function of level splitting ( $\Delta$ ) for  $J/U = 0.0$  and  $\Gamma_{\pm}/U = \Gamma/U = 0.4$ .

levels  $i = \pm$  becomes unequal even for  $\Delta = \epsilon_+ - \epsilon_- = 0$ ,  $\langle n_+ \rangle \neq \langle n_- \rangle$ . This phenomenon is similar to the spontaneous moment formation found by Anderson,<sup>35,55</sup> which we eliminated here by setting the Green's functions explicitly proportional to  $\sim \delta_{\sigma\sigma'}$ . In a perturbative calculation one should always stay away from these regions in parameter space to avoid spurious solutions. Fortunately, as shown in Fig. 3, we can easily identify these "dangerous" regions by computing the occupation numbers  $\langle n_{\pm} \rangle$  as a function of level splitting,  $\Delta/U$ , since  $\langle n_{\pm} \rangle$  exhibit hysteresis there.

Carrying out a similar hysteresis analysis for each value of the parameters  $U/\Gamma$  and  $J/\Gamma$ , we obtain the stability diagram, Fig. 4, delineating the region of applicability of our perturbative approach (for simplicity, here we took  $\Gamma_{\pm} = \Gamma$ ). Clearly, one needs to keep both  $U/\Gamma$  and  $J/\Gamma$  moderate to stay within the range of applicability of iterative perturbation theory.

### III. RESULTS AND DISCUSSION

#### A. The symmetric case ( $\Gamma_+ = \Gamma_-$ )

The parameter space of the two-level quantum dot is huge. Therefore, to get more intuition, we first restrict somewhat the number of independent parameters by assuming that both levels couple to the leads with equal strength,  $\Gamma_{\pm} \equiv \Gamma$ . We assume further that the dot is at the particle-hole symmetrical point,  $\epsilon_+ = -\epsilon_- = \Delta/2$ , where the number of electrons on the dot is fixed to  $n = \sum_{i,\sigma} \langle n_{i\sigma} \rangle = 2$ . Before presenting the numerical data, let us briefly discuss the structure of the ground state as a function of  $J$ ,  $U$ , and  $\Delta$  in case of small tunnelings,  $\Gamma$ .

In the absence of tunneling to the leads,  $\Gamma = 0$ , the states of the dot can be grouped into three singlets (with spin  $S = 0$ ) and a triplet ( $S = 1$ ). Two singlet

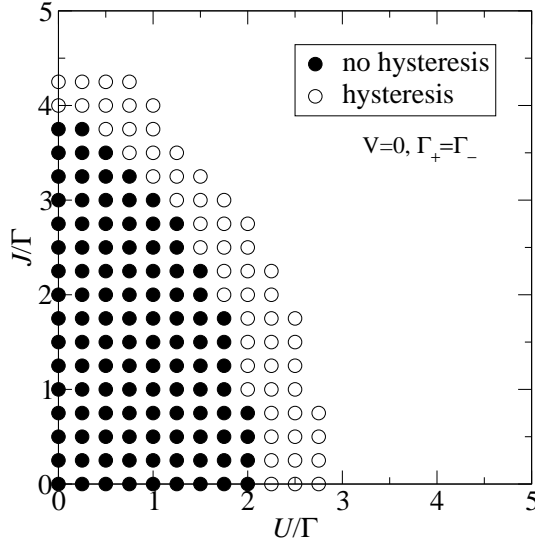


FIG. 4: Stability region of perturbation theory for  $\Gamma = \Gamma_{\pm}$ . Empty circles mark the region of hysteresis, while filled circles indicate the stable region, where PT gives meaningful results.

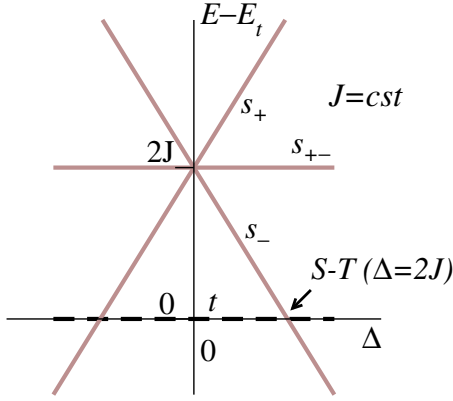


FIG. 5: Evolution of the singlet and triplet states of the isolated dot for fixed  $J > 0$ , as a function of  $\Delta$ . Energies are measured from the energy  $E_t$  of the triplet state. The singlet-triplet transition point is also indicated (S-T).

states,  $|s_{\pm}\rangle$  correspond to putting two electrons on the upper/lower level, while a third state,  $|s_{+-}\rangle$ , is a singlet with one electron residing on each level. The rest of the two-electron states are spanned by a triplet state,  $|t, m\rangle$  ( $m = 0, \pm$ ), where the spin of the electron on level  $i = +$  is aligned with that on level  $i = -$ . Fig. 5 shows the evolution of these four levels as a function of the splitting  $\Delta$  for finite  $J$ . For  $\Delta = 0$  the triplet state is the ground state, and the three singlet states form degenerate excited states of energy  $2J$ . Increasing  $\Delta$ , however, pulls down the state  $|s_{-}\rangle$ , which becomes the ground state for  $\Delta > 2J$ .

This picture is slightly modified if the dot is coupled to the leads. In this case, for generic couplings,<sup>43,56</sup> the transition becomes a smooth cross-over, so that the

triplet and singlet states are adiabatically connected. However, the various regimes are described by rather different physical pictures. For large values of  $\Delta$ , the two dot electrons form a local singlet on the dot, while for  $J \ll |\Delta|$  they are aligned into a triplet, which then couples to the leads through an exchange coupling, and is screened by a two-stage Kondo effect for  $\Gamma_{+} < \Gamma_{-}$  at some temperatures  $T_K^{+} < T_K^{-}$ . In this regard, the case  $\Gamma_{-} \equiv \Gamma_{+}$  is rather special, since then only a single Kondo scale appears,  $T_K^{+} = T_K^{-}$ . As one approaches the transition region,  $\Delta \approx 2J$ , from the triplet side, the Kondo temperatures  $T_K^{\pm}$  increase, until the singlet state  $s_{-}$  and the triplet states are all inseparably mixed into a single quantum state, characterized by a Fermi liquid scale,  $T_K^{*}$ .<sup>57,58</sup> These three regions are sketched in Fig. 6.

### 1. Spectral functions

To gain insight to the effects governing the conductance through the dot, it is useful to study first the equilibrium spectral functions.

*Case of no Hund's rule coupling,  $J \equiv 0$ .* Let us first investigate in the absence of Hund's rule coupling,  $J \equiv 0$ . In this case, there is no triplet region, rather, changing  $\Delta$ , one finds a transition between the two singlet states  $|s_{-}\rangle \rightarrow |s_{+}\rangle$  through a peculiar Kondo state formed by all three singlet states and the triplet (see Fig. 5). Fig. 7 shows the total spectral function,  $\rho_T(\omega)$ , in this case, for  $\Gamma/U = 0.565$ , as a function of level splitting,  $\Delta/U$ .

For  $\Delta/U = 0$  and  $J/U = 0$ , the ground state of an isolated dot is sixfold degenerate. When the quantum dot is connected to the leads, a strong Kondo resonance driven by the quantum fluctuations of this sixfold degenerate state appears at  $\omega = 0$ . The width of this peak can be identified as the Kondo temperature,  $T_K^{*}$ . In addition, one observes two shoulders at  $\omega \approx \pm U$ , which can be identified as the Hubbard peaks.

Increasing  $\Delta$  first slightly suppresses the Kondo resonance at  $\omega = 0$ , and finally, for  $\Delta > T_K^{*}$  splits the resonance into two side-peaks. These side-peaks can be identified as the singlet-triplet excitation peaks, and their position can be precisely determined from the level-projected spectral functions,  $\rho_{\pm}(\omega)$ . As shown in the inset of Fig. 7, for large values of  $\Delta$  they are indeed

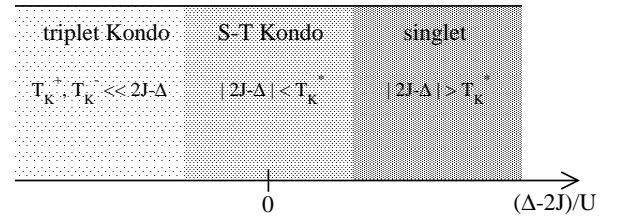


FIG. 6: Sketch of the singlet, triplet, and transition regimes, as a function of  $\Delta/U$  for a fixed  $J > 0$ .

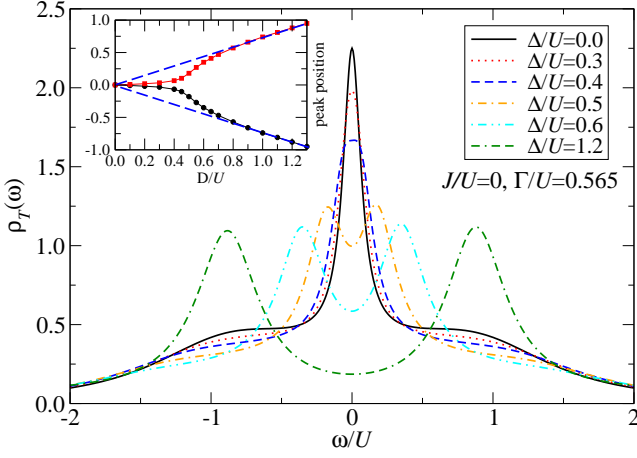


FIG. 7: Total equilibrium spectral functions,  $\rho_T(\omega)$ , for  $J/U = 0$  and  $\Gamma_\pm/U = \Gamma/U = 0.565$ , and different values of the level splitting,  $\Delta/U$ . Inset: Evolution of the peak positions in  $\rho_\pm(\omega)$  as a function of  $\Delta/U$ . The dashed lines indicate  $\omega = \pm\Delta$ .

located at  $\omega \approx \pm\Delta$ , although the splitting takes place rather abruptly at  $\Delta \approx 0.4$ , and the  $\Delta$ -dependence of the maxima of  $\rho_\pm(\omega)$  is very non-linear.

*Finite Hund's rule coupling,  $J > 0$ .* The effect of the level splitting  $\Delta$  on the equilibrium spectral function is presented in Fig. 8 for parameters  $J/U = 0.2$  and  $\Gamma/U = 0.565$ . The spectral functions behave quite similarly to those calculated for  $J = 0$ : A Kondo resonance appears for  $\Delta = 0$  in  $\rho_T(\omega)$ , which is gradually suppressed as  $\Delta$  increases, and finally splits into two resonances for large values of  $\Delta$ . However, in this case, we should interpret the Kondo resonance slightly differently than before. For  $\Delta = 0$  the ground state of the iso-

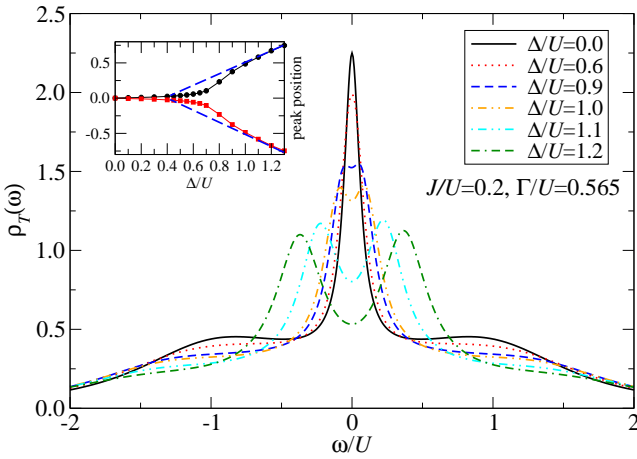


FIG. 8: Total equilibrium spectral functions,  $\rho_T(\omega)$ , for  $J/U = 0.2$ ,  $\Gamma_\pm/U = \Gamma/U = 0.565$ , for different values of level splitting,  $\Delta/U$ . Inset: Peak positions of  $\rho_\pm(\omega)$  as a function of  $\Delta/U$ . The dashed lines indicate  $\omega = \pm(\Delta - 2J)$ .

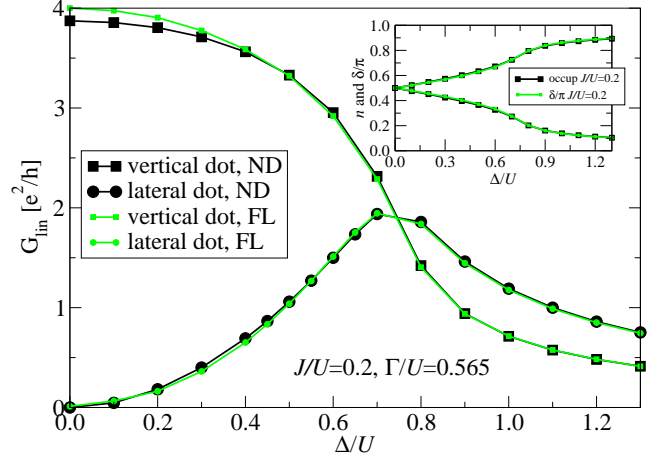


FIG. 9: Linear conductance of lateral and vertical dots for  $J/U = 0.2$ , from numerical derivation (ND) of the current at zero bias, and from the Fermi liquid relations (FL). Inset: Comparison of occupation numbers and phase shifts,  $\delta/\pi$ . The conductance of a symmetrical lateral dot shows a maximum of height  $2e^2/h$  around the ST transition.

lated dot would be a triplet state, and therefore turning on a small  $\Gamma$ , this spin triplet gets screened by the conduction electrons in the leads through a *triplet Kondo effect*.<sup>59</sup> Although  $\Gamma$  is relatively large in our case and comparable to the singlet triplet splitting,  $\Gamma \sim 2J$ , nevertheless, this interpretation still holds, since the width of the central resonance ( $T_K$ ) is still smaller than the splitting  $\Delta E_{st} \equiv |\Delta - 2J|$ . In fact, the resonance splits approximately where  $\Delta E_{st} \sim T_K$ , and the positions of the split resonances follow approximately the straight lines  $\omega \approx \pm(\Delta - 2J)$  for large  $\Delta$ 's (see the inset of Fig. 8), in complete agreement with the ST transition picture.

## 2. Conductance

Having investigated the equilibrium spectral functions, let us now turn to the discussion of non-equilibrium transport through the dot. We first focus on the *linear conductance*,  $G_{\text{lin}} = dI/dV|_{V=0}$ . This is plotted in Fig. 9 as a function of  $\Delta$  both for lateral and vertical dots with a finite Hund's rule coupling,  $J/U = 0.2$ . We computed  $G_{\text{lin}}$ , on one hand, by numerically differentiating the current, Eq. (25), but we also computed it by extracting the phase shifts from the retarded Green's functions and the occupation numbers, and then using the Landauer-Büttiker formula (Eq. (30) for lateral and Eq. (31) for vertical dots). As shown in Fig. 9, the two procedures give identical results within numerical accuracy.

Vertical and lateral dots exhibit very different characteristics. The linear conductance of a lateral dot shows a maximum around the ST transition and it is small on both sides of the transition, while the conductance of a vertical dot crosses over smoothly from a conductance of  $G_{\text{lin}} \approx 4e^2/h$  at  $\Delta = 0$  to a small value for



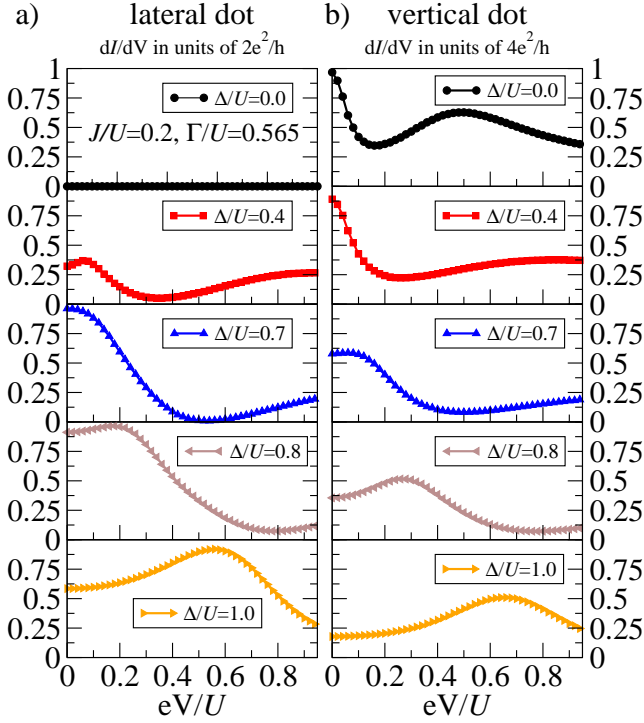


FIG. 10: Differential conductance,  $G(V)$ , for  $J/U = 0.2$  and  $\Gamma_{\pm}/U = \Gamma/U = 0.565$  for different level splittings,  $\Delta/U$  both for lateral (a) and for vertical (b) quantum dots. For vertical dots the suppression and the splitting of the Kondo resonance are clearly visible in  $G(V)$ . For lateral dots, interference effects mask the signal on the triplet side.

$\Delta \gg 2J$ . This behavior can be understood from Eqs. (30) and (31), and the behavior of the phase shifts, shown in the inset of Fig. 9: In the triplet regime,  $\Delta \approx 0$ , two conduction electrons are needed to screen the local spin  $S = 1$ . Therefore, both phase shifts are close to  $\delta_{\pm} \approx \pi/2$  by the Friedel sum rule.<sup>13</sup> While for a vertical dot the contributions of the channels  $i = \pm$  add up to the conductance, and amount in a total conductance of  $G_{\text{lin}} = 4e^2/h$ , for lateral dots there is a destructive interference (see Eq. 30), which finally amounts in a complete back-reflection of electrons and no conductance,  $G \approx 0$ .<sup>44,49,56</sup> Increasing  $\Delta$ , the phase shifts gradually cross over to values,  $\delta_- \approx \pi$  and  $\delta_+ \approx 0$ . This gives rise to a maximal conductance of  $G_{\text{lin}} = 2e^2/h$  somewhere in the vicinity of the ST transition for a lateral dot,<sup>49</sup> while it results in the monotonous decrease of the conductance of a vertical dot,<sup>59</sup> as shown in Fig. 9. The Friedel sum rule, Eq. (29), is verified in the inset of Fig. 9, where we compare the phase shifts to the occupation numbers.

The differential conductance,  $G(V)$ , can be observed in Fig. 10. For a vertical dot, the behavior of  $G(V)$  follows the naive expectations based upon the spectral functions' structure and the excitation spectra of the dots: For  $\Delta = 0$  a clear Kondo resonance is seen at  $V \approx 0$ , and the singlet excitations give a broad resonance at  $V \approx 2J/e$ . Increasing  $\Delta$ , the central resonance is suppressed in am-

plitude (as predicted by the Friedel sum rule), but it also broadens somewhat as one approaches the ST transition point, where quantum fluctuations give rise to a somewhat higher Kondo temperature,  $T_K^*$ .<sup>57,58</sup> The excitation peak at  $V \approx (2J - \Delta)/e$  shifts to lower energies and gradually merges with the central resonance. Finally, for  $\Delta > 2J$  the quantum dot is in the singlet region. There the central resonance splits up and a resonance is observed at  $V \approx (\Delta - 2J)/e$ .

While it is easy to understand the differential conductance of a vertical dot, the conductance of a lateral dot is counter-intuitive. For  $\Delta = 0$  there is a complete destructive interference, and  $G(V) \equiv 0$ . We emphasize that this is only valid for the symmetrical case,  $\Gamma_+ = \Gamma_-$ , studied in this section. Increasing  $\Delta$ ,  $G(V)$  becomes non-zero, and the conductance gradually increases. The shape of  $G(V)$ , however, does not have a simple intuitive explanation on the triplet side of the transition, as a result of the cancellation of the various contributions. Around the transition point and beyond that ( $\Delta > 2J$ ), however, the phase shifts are far away from  $\pi/2$ , interference effects are suppressed, and the conductance shows features which are quite similar to those found for vertical dots, discussed above.

### B. The asymmetric case, $\Gamma_+ \neq \Gamma_-$

In the previous subsection, we analyzed the case of equal tunneling rates,  $\Gamma_+ = \Gamma_-$ . While this assumption may be a good approximation for some systems (for carbon nanotubes, e.g.),<sup>1</sup> it is violated for most quantum dots.<sup>41,42</sup> Let us therefore investigate in this subsection the generic case of unequal couplings,  $\Gamma_+ \neq \Gamma_-$ . The range of applicability of our perturbative method is shown in Fig. 11. For simplicity, we fixed  $\Gamma_+ = \Gamma_-/2$  throughout this subsection, and characterized the hybridization strength in terms of the geometric mean of  $\Gamma_{\pm}$ ,  $\Gamma \equiv \sqrt{\Gamma_+ \Gamma_-}$ . A comparison of Fig. 11 and Fig. 4 shows that the range of applicability of perturbation theory is only weakly modified by the asymmetry in the tunneling rates.

For  $\Gamma_+ \neq \Gamma_-$ , a few important differences appear though compared to the case of equal tunneling strengths. When  $\Gamma_+ \neq \Gamma_-$ , the particle-hole symmetry, Eq. (13), of the Hamiltonian is not valid anymore. As a consequence, the number of electrons on the dot is not exactly two and the spectral functions also violate the electron-hole symmetry relation, and  $\varrho_+(\omega) \neq \varrho_-(-\omega)$ . Electron-hole symmetry is only maintained for  $\Delta = 0$ , where  $\varrho_+(\omega) = \varrho_+(-\omega)$  and  $\varrho_-(\omega) = \varrho_-(-\omega)$  follow from the second electron-hole symmetry transformation, Eq. (14). The second major difference is that, due to the two different coupling strengths, two separate Kondo scales emerge for the even and odd channels on the triplet side,  $T_K^{\pm}$ .<sup>41</sup>

Both differences are clearly visible in the spectral functions, shown in Fig. 12, where the level-projected spectral

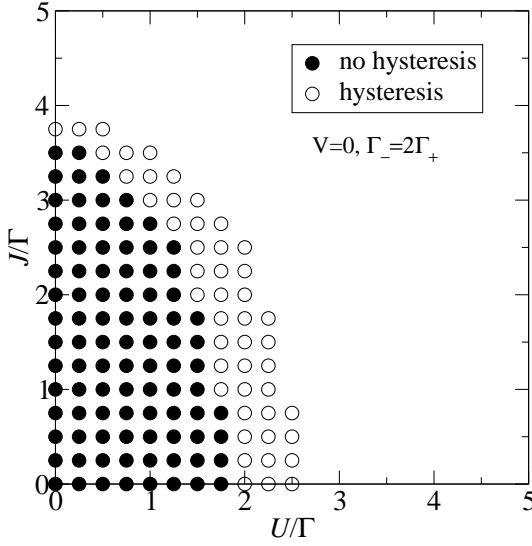


FIG. 11: Range of applicability of perturbation theory for  $\Gamma_+ \neq \Gamma_-$ , as extracted from the hysteresis of occupation numbers. Filled circles indicate the region of stable perturbation theory. Couplings are measured in units of  $\Gamma \equiv \sqrt{\Gamma_+ \Gamma_-}$ .

functions are also displayed. Clearly, only the  $\Delta = 0$  spectral functions are electron-hole symmetrical, and even there, the spectral functions  $\rho_+$  and  $\rho_-$  have a central Kondo resonance of different width.

Apart from these differences, the overall evolution of the spectral functions as well as that of the phase shifts (see inset of Fig. 13) is quite similar to the one observed for  $\Gamma_+ = \Gamma_-$ . As a result, the behavior of the linear conductance as a function of the level splitting,  $\Delta$ , is also quite similar to the one obtained for  $\Gamma_+ = \Gamma_-$  (see Fig. 13).

The *differential conductance* is, however, quite different, and shows a much richer structure on the triplet side in this case. For  $\Delta = 0$ , both phase shifts are pinned to  $\delta_{\pm} = \pi/2$  by electron-hole symmetry. The physical reason for this is, of course the formation of a Fermi liquid state through a Kondo effect in both channels on the triplet side. As a consequence, by Eq. (30), the linear conductance vanishes also in this case,  $G(V=0) = 0$ . As we emphasized earlier, this result is due to an interference between the channels,  $i = \pm$ . However, for a voltage in the range,  $T_K^+ < eV < T_K^-$ , the Kondo effect in channel  $i = +$  is destroyed, while the Kondo effect is still well-developed in channel  $i = -$ . As a result, the destructive interference is suppressed as one turns on the voltage, and the conductance becomes non-zero. For even larger voltages,  $T_K^- < eV$ , the Kondo effect is also destroyed in channel  $i = -$ , and the differential conductance starts to decrease with increasing voltage. Thus the result of the consecutive destruction of the two Kondo effects is the appearance of a peak at  $eV \approx T_K^+$ .<sup>43,44,56</sup> This signature of the two-stage Kondo effect is clearly visible in the differential conductance,  $G(V)$ , shown in Fig. 14. There not only the central resonance-antiresonance structure can be

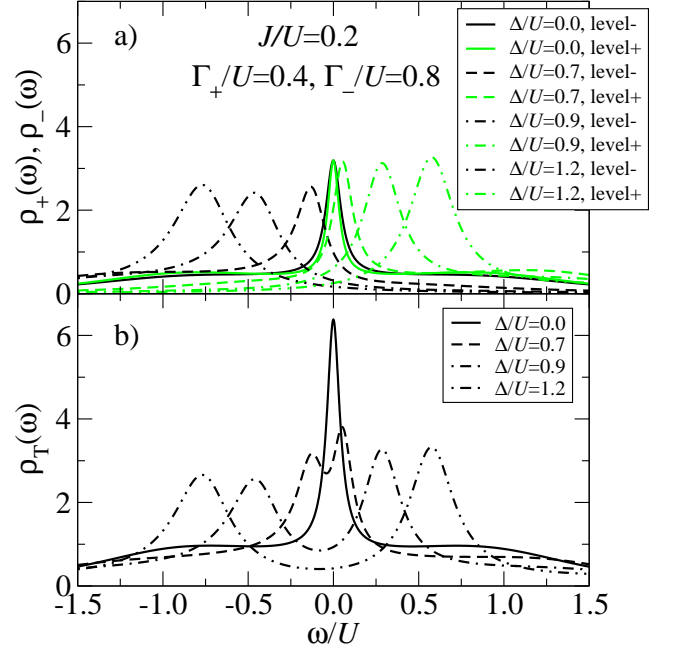


FIG. 12: Spectral functions for  $J/U = 0.2$ ,  $\Gamma_+/U = 0.4$  and  $\Gamma_-/U = 0.8$ , for different values of level splitting,  $\Delta/U$ . The upper panel shows the level-projected spectral functions,  $\rho_{\pm}(\omega)$ , while in the lower panel the full spectral functions,  $\rho_T(\omega)$ , are presented. Notice the breaking of electron-hole symmetry for any  $\Delta \neq 0$ .

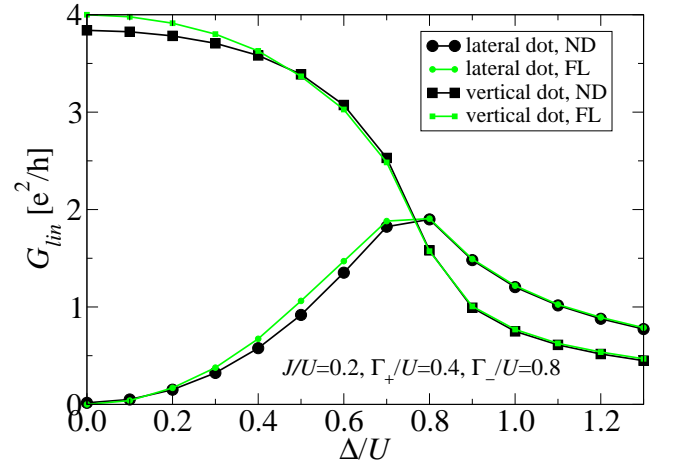


FIG. 13: Linear conductance for  $J/U = 0.2$ ,  $\Gamma_+/U = 0.4$  and  $\Gamma_-/U = 0.8$ , as obtained from numerical derivation of the current (ND), and from the Fermi liquid relations (FL). The inset shows the phase shifts  $\delta_{\pm}/\pi$  extracted from the Green's functions at  $\omega = 0$ , and the occupation numbers,  $n_{\pm}$ .

seen, but also, a side-resonance at  $\omega \approx 2J$ , which can be associated with the singlet excitations.

As shown in Fig. 15, for the lateral dot, increasing  $\Delta$  gradually fills up the central dip, until the two resonances merge into a single ST-Kondo peak at around  $\Delta \approx 2J$ , and finally split to two peaks located at  $eV \approx \pm(\Delta - 2J)$ . All these features are in excellent agreement with the

experimental results of van der Wiel *et al.*,<sup>41</sup> and Granger *et al.*, (see Fig. 3e in Ref. 42).

In Fig. 15 we also present our results for the differential conductance through a vertical dot. Contrary to the differential conductance of the lateral dot, these  $G(V)$  curves do not exhibit any remarkable difference with respect to the curves in Fig. 10, obtained for  $\Gamma_+ = \Gamma_-$ . The main reason for this is that the perturbative approach does not estimate correctly the Kondo temperature: while for a non-perturbative calculation one would expect  $T_K^+ \ll T_K^-$  for the couplings used, perturbation theory gives Kondo temperatures,  $T_K^\pm$ , of the same order of magnitude. While this is sufficient to produce a visible effect in the differential conductance of a lateral dot, it is not sufficient to see the expected two-peak structure in the differential conductance of a vertical dot. In fact, for  $T_K^+ \ll T_K^-$ , the conductance should display two resonances on the top of each other, a narrow one of width  $\Delta V \sim T_K^+/e$  and a broad one of width  $\Delta V \sim T_K^-/e$ , both of height  $\Delta G \approx 2e^2/h$ . However, since  $T_K^+ \sim T_K^-$  in our calculation, these two peaks merge into a single resonance of height  $4e^2/h$  on the triplet side of the transition.

Our theoretical results for the vertical dots can be compared to the experimental curves of Sasaki *et al.*<sup>50</sup> The evolution of the differential conductance on the singlet side of the transition and at the crossover point shows similarity with the experiments, but the data of Sasaki *et al.* do not display the three-peak structure expected on the triplet side. The reason for this is that, the experiments were performed at a finite temperature: the Kondo temperatures  $T_K^\pm$  on the triplet side sink very quickly below the temperature as one gets farther away from the S-T degeneracy point, and therefore the central Kondo resonance was unobservable.

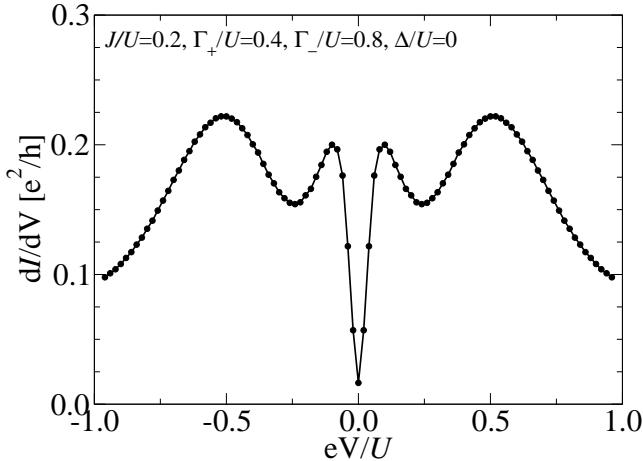


FIG. 14: Differential conductance of a lateral quantum dot for  $J/U = 0.2$ ,  $\Gamma_+/U = 0.4$ , and  $\Gamma_-/U = 0.8$ , for level splitting  $\Delta/U = 0$ . The side-peak can be attributed to the singlet excitation energy,  $2J$ , while the central resonance-antiresonance structure is associated with the two consecutive Kondo effects on the triplet side.

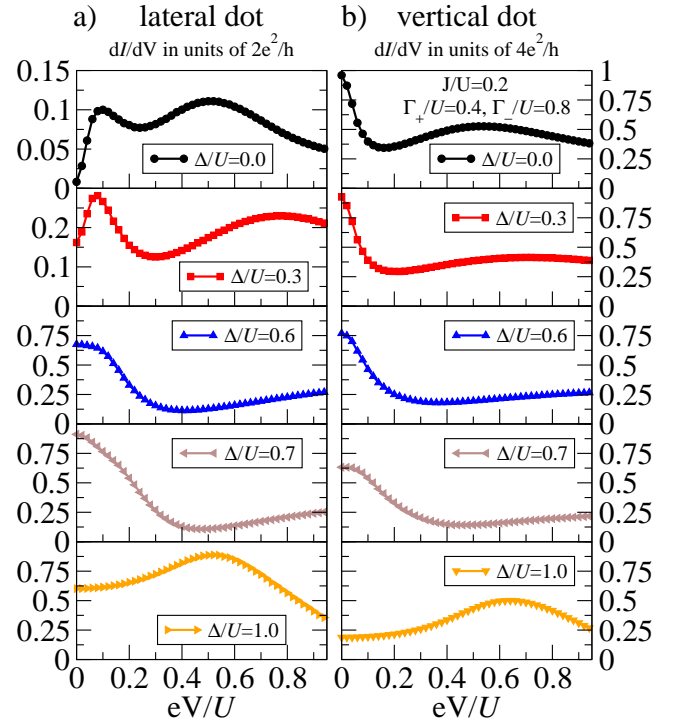


FIG. 15: Differential conductance,  $G(V)$ , for  $J/U = 0.2$ ,  $\Gamma_+/U = 0.4$  and  $\Gamma_-/U = 0.8$  for different level splittings,  $\Delta/U$  for a lateral (a) and a vertical (b) quantum dot. The two consecutive Kondo resonances on the triplet side are clearly visible in the lateral dot (middle resonance-antiresonance structure), while the two Kondo resonances merge into a single peak in a vertical dot.

#### IV. CONCLUSIONS

In this paper, we studied the non-equilibrium singlet triplet transition in lateral and in vertical quantum dots. We described the quantum dots in terms of a simple two-level Anderson model, which included the Hund's rule coupling ( $J$ ) as well as the charging energy of the dot ( $U$ ), and we used non-equilibrium iterative perturbation theory to describe the transport through the dot.

As a first step, we explored the range of validity of perturbation theory and found that it breaks down at intermediate coupling strengths, where multiple solutions and hysteresis appear as an indication of spontaneous orbital polarization formation. Then we computed the equilibrium spectral functions, determined the non-equilibrium Green's functions, and finally used the Meir-Wingreen formula to compute the differential conductance through the dot.

To our great surprise, within its range of validity, this simple approach is able to describe essentially *all experimentally-observed properties* of the transition. In particular, for a lateral dot with level-dependent decay rates,  $\Gamma_\pm$ , the differential conductance,  $G(V)$ , displays the correct resonance-antiresonance structure corresponding to the two-stage Kondo effect on the triplet

side, while in the vicinity of the S-T transition these two resonances merge with the singlet excitation into a single Kondo resonance. On the singlet side of the transition we find a split Kondo resonance, and we recover the correct location of the side peaks,  $eV \approx \pm(\Delta - 2J)$ .

For a lateral dot, the linear conductance,  $G_{\text{lin}}(\Delta)$  exhibits a broad maximum of height  $G_{\text{max}} = 2e^2/h$  around the transition, which is located at the correct level splitting,  $\Delta \approx 2J$ . On the other hand, for a vertical dot we find a maximal linear conductance of  $4e^2/h$  on the triplet side of the transition, which gradually crosses over to a small conductance on the singlet side. We also verified that our numerical calculations satisfy the Friedel sum rule, and that the linear conductance as computed by numerical differentiation of the Meir-Wingreen formula is identical to the one computed from the phase shifts using the Landauer-Büttiker formula (assuming a Fermi liquid ground state).

The differential conductance of a vertical dot also behaves in the correct way: A Kondo resonance (double resonance) is found on the triplet side, which is suppressed and broadened around the transition, and finally splits into two resonances on the singlet side.

We thus arrive at the remarkable and surprising conclusion that the perturbative approach is able to describe this rather complex behavior, and is in rather good agreement with the experiments. It has however, some important limitations: (1) Its range of validity is limited to small and intermediate couplings, and (2) it is unable to account for the correct width of the Kondo resonance. Furthermore, though we checked that our solutions satisfy current conservation, simple perturbation theory is not a conserving approximation, and in general a lot of care must be taken to satisfy it. However, as we show in a consecutive paper,<sup>47</sup> the problem of the width of the Kondo resonance as well as that of current conservation can be overcome at the expense of getting somewhat poorer resolution of the Hubbard peaks by using the method of fluctuation exchange approximation.<sup>47,60</sup>

Acknowledgement: This research has been supported by Hungarian grants OTKA No. K73361 and OTKA NN76727, the EU GEOMDISS project and its NKTH

supplementary funding, OMFB-00292/2010, and the Romanian grant CNCSIS PN II ID-672/2009.

## Appendix A: Hybridized non-interacting Green's functions

For completeness, here we enumerate the non-interacting Green's functions,  $\mathbf{g}$ . They can be easily constructed based on the Dyson equation

$$\mathbf{g}^{-1}(\omega) = \mathbf{g}_0^{-1}(\omega) - \Sigma_{\Gamma}(\omega), \quad (\text{A1})$$

where we used the matrix notation of the main text. The Green's functions,  $\mathbf{g}_0$ , in Eq. (A1) denote the Green's functions of the isolated dot, with energies replaced by the effective energies,  $\tilde{\varepsilon}_{i\sigma}$ , and its matrix elements are given by

$$g_0^{\kappa\kappa' -1}_{i\sigma, i'\sigma'} = s_{\kappa} \delta_{ii'} \delta_{\sigma\sigma'} \delta_{\kappa\kappa'} (\omega - \tilde{\varepsilon}_{i\sigma}), \quad (\text{A2})$$

with  $s_{\kappa}$  the Keldysh sign defined in the main text. The self-energy,  $\Sigma_{\Gamma}$ , denotes the self-energy coming from the hybridization of the dot and the leads, and its matrix elements can be computed in terms of the tunneling matrix elements,  $t_{i\alpha}$ ,

$$\begin{aligned} \Sigma_{\Gamma}^T{}_{i\sigma, i'\sigma'} &= i \pi \delta_{\sigma\sigma'} \sum_{\alpha=L,R} t_{i\alpha} t_{i'\alpha} (2f_{\alpha}(\omega) - 1), \\ \Sigma_{\Gamma}^<{}_{i\sigma, i'\sigma'} &= -i 2\pi \delta_{\sigma\sigma'} \sum_{\alpha=L,R} t_{i\alpha} t_{i'\alpha} f_{\alpha}(\omega), \\ \Sigma_{\Gamma}^>{}_{i\sigma, i'\sigma'} &= -i 2\pi \delta_{\sigma\sigma'} \sum_{\alpha=L,R} t_{i\alpha} t_{i'\alpha} (f_{\alpha}(\omega) - 1), \\ \Sigma_{\Gamma}^{\bar{T}}{}_{i\sigma, i'\sigma'} &= i \pi \delta_{\sigma\sigma'} \sum_{\alpha=L,R} t_{i\alpha} t_{i'\alpha} (2f_{\alpha}(\omega) - 1), \end{aligned}$$

with  $f_{\alpha}(\omega)$  denoting the chemical potential-shifted Fermi functions of the leads. In the numerical calculations, we inverted numerically Eq. (A1) to obtain  $\mathbf{g}$ .

<sup>1</sup> N. Roch, S. Florens, V. Bouchiat, W. Wernsdorfer and F. Balestro, *Nature* **453**, 633 (2008).

<sup>2</sup> N. Roch, S. Florens, T. A. Costi, Wolfgang Wernsdorfer and Franck Balestro, *Phys. Rev. Lett.* **103**, 197202 (2009);

<sup>3</sup> K. Moth-Poulsen, T. Bjørnholm, *Nature Nanotechnology* **4**, 551 (2009).

<sup>4</sup> J. J. Parks, A. R. Champagne, T. A. Costi, W. W. Shum, A. N. Pasupathy, E. Neuscamman, S. Flores-Torres, P. S. Cornaglia, A. A. Aligia, C. A. Balseiro, G. K.-L. Chan, H. D. Abruna and D. C. Ralph, *Science* **328**, 1370 (2010).

<sup>5</sup> R. Hanson, L. P. Kouwenhoven, J. R. Petta, S. Tarucha and L. M. K. Vandersypen, *Rev. Mod. Phys.* **79**, 1217 (2007).

<sup>6</sup> M. Grobis, I.G. Rau, R.M. Potok, and D. Goldhaber-

Gordon. "Kondo Effect in Mesoscopic Quantum Dots", *Handbook of Magnetism and Magnetic Materials*, H. Kronmüller and S. Parkin, eds., (Wiley, 2007).

<sup>7</sup> J. R. Heath, *Annu. Rev. Mater. Res.* **39**, 1 (2009).

<sup>8</sup> D. Loss and D. P. DiVincenzo, *Phys. Rev. A* **57**, 120 (1998).

<sup>9</sup> J. Martinek, M. Sindel, L. Borda, J. Barnas, J. König, G. Schön and J. von Delft, *Phys. Rev. Lett.* **91**, 247202 (2003).

<sup>10</sup> M. R. Calvo, J. Fernandez-Rossier, J. J. Palacios, D. Jacob, D. Natelson and C. Untiedt, *Nature* **458**, 1150 (2009).

<sup>11</sup> M.-S. Choi, M. Lee, K. Kang and W. Belzig, *Phys. Rev. B* **70**, 020502 (2004).

<sup>12</sup> P. Jarillo-Herrero, J. A. van Dam and L. P. Kouwenhoven,



- Nature **439**, 953 (2006).
- <sup>13</sup> J. Bauer, A. Oguri and A. C. Hewson, J. Phys.: Cond. Mat. **19**, 486211 (2007);
  - <sup>14</sup> L. Hofstetter, S. Csonka, J. Nygard and C. Schönenberger, Nature **461**, 960 (2009).
  - <sup>15</sup> R.M. Potok, I.G. Rau, H. Shtrikman, Y. Oreg and D. Goldhaber-Gordon, Nature **446**, 167 (2006).
  - <sup>16</sup> M. Vojta, R. Bulla, and W. Hofstetter, Phys. Rev. B **65** 140405 (2002).
  - <sup>17</sup> A. Kogan, G. Granger, M. A. Kastner, D. Goldhaber-Gordon and H. Shtrikman, Phys. Rev. B **67** 113309 (2003).
  - <sup>18</sup> G. Zaránd, C.-H. Chung, P. Simon and M. Vojta, Phys. Rev. Lett. **97**, 166802 (2006).
  - <sup>19</sup> E. Sela and I. Affleck, Phys. Rev. Lett. **102**, 047201 (2009).
  - <sup>20</sup> J. Eckel, F. Heidrich-Meisner, S. G. Jakobs, M. Thorwart, M. Pletyukhov and R. Egger, New. J. Phys. **12**, 043042 (2010).
  - <sup>21</sup> J. E. Han, Phys. Rev. B **81**, 245107 (2010).
  - <sup>22</sup> P. Mehta and N. Andrei, Phys. Rev. Lett **96**, 216802 (2006).
  - <sup>23</sup> See also the correction in: P. Mehta, S. P. Chao and N. Andrei, arXiv:cond-mat/0703426 (2007).
  - <sup>24</sup> E. Boulat, H. Saleur and P. Schmitteckert, Phys. Rev. Lett. **101**, 140601 (2008).
  - <sup>25</sup> A. Rosch, J. Paaske, J. Kroha, and P. Wölfe, J. Phys. Soc. Japan **74**, 118 (2005); A. Rosch, J. Paaske, J. Kroha and P. Wölfe, Phys. Rev. Lett. **90**, 076804 (2003).
  - <sup>26</sup> S. G. Jakobs, M. Pletyukhov and H. Schoeller, Phys. Rev. B **81**, 195109 (2010).
  - <sup>27</sup> M. Moeckel, S. Kehrein, Ann. Phys. **324**, 2146 (2009).
  - <sup>28</sup> S. Andergassen, V. Meden, H. Schoeller, J. Splettstoesser and M. R. Wegewijs, arXiv:cond-mat/1005.1187 (2010).
  - <sup>29</sup> F. B. Anders and A. Schiller, Phys. Rev. Lett. **95**, 196801 (2005).
  - <sup>30</sup> U. Schollwöck, Rev. Mod. Phys. **77**, 259 (2005).
  - <sup>31</sup> A. Levy Yeyati, A. Martín-Rodero, and F. Flores, Phys. Rev. Lett. **71**, 2991 (1993).
  - <sup>32</sup> H. Kajueter and G. Kotliar, Phys. Rev. Lett. **77**, 131 (1996).
  - <sup>33</sup> A. A. Aligia, Phys. Rev. B **74**, 155125 (2006).
  - <sup>34</sup> K. S. Thygesen and A. Rubio, Phys. Rev. B **77**, 115333 (2008).
  - <sup>35</sup> B. Horváth, B. Lazarovits, O. Sauret, and G. Zaránd, Phys. Rev. B **77**, 113108 (2008).
  - <sup>36</sup> G. Zaránd, A. Brataas and D. Goldhaber-Gordon, Solid State Commun. **126**, 463 (2003).
  - <sup>37</sup> L. Borda, G. Zaránd, W. Hofstetter, B. I. Halperin, and J. von Delft, Phys. Rev. Lett. **90**, 026602 (2003).
  - <sup>38</sup> S. Sasaki, S. Amaha, N. Asakawa, M. Eto and S. Tarucha, Phys. Rev. Lett. **93**, 017205 (2004).
  - <sup>39</sup> P. Jarillo-Herrero, J. Kong, H. S. J. van der Zant, C. Dekker, L. P. Kouwenhoven and S. De Franceschi, Nature **434**, 484 (2005).
  - <sup>40</sup> M.-S. Choi, R. López and R. Aguado, Phys. Rev. Lett. **95**, 067204 (2005).
  - <sup>41</sup> W. G. van der Wiel, S. De Franceschi, J. M. Elzerman, S. Tarucha, L. P. Kouwenhoven, J. Motohisa, F. Nakajima, and T. Fukui, Phys. Rev. Lett. **88**, 126803. (2002).
  - <sup>42</sup> G. Granger, M. A. Kastner, Iuliana Radu, M. P. Hanson and A. C. Gossard, Phys. Rev. B **72**, 165309 (2005).
  - <sup>43</sup> M. Pustilnik and L. I. Glazman, Phys. Rev. Lett. **87**, 216601 (2001).
  - <sup>44</sup> W. Hofstetter and G. Zaránd, Phys. Rev. B **69**, 235301 (2004).
  - <sup>45</sup> P. Roura Bas and A. A. Aligia, J. Phys.: Condens. Matt. **22**, 025602 (2010).
  - <sup>46</sup> J. Paaske, A. Rosch, P. Wölfe, N. Mason, C. M. Marcus and J. Nygard, Nature Physics **2**, 460 (2006).
  - <sup>47</sup> B. Horváth et al. (unpublished)
  - <sup>48</sup> M. Pustilnik and L. I. Glazman, Phys. Rev. B **64**, 045328 (2001).
  - <sup>49</sup> M. Pustilnik and L. I. Glazman, Phys. Rev. Lett. **85**, 2993 (2000).
  - <sup>50</sup> S. Sasaki, S. De Franceschi, J. M. Elzerman, W. G. van der Wiel, M. Eto, S. Tarucha and L. P. Kouwenhoven, Nature **405**, 764 (2000).
  - <sup>51</sup> J. Nygard, D. H. Cobden and P. E. Lindelof, Nature **408**, 342 (2000).
  - <sup>52</sup> J. Rammer and H. Smith, Rev. Mod. Phys. **58**, 323 (1986).
  - <sup>53</sup> Y. Meir and N. S. Wingreen, Phys. Rev. Lett. **68**, 2512 (1992).
  - <sup>54</sup> A. C. Hewson, *The Kondo Problem to Heavy Fermions* (Cambridge University Press, Cambridge, 1993).
  - <sup>55</sup> P. W. Anderson, Phys. Rev. **124**, 41 (1961).
  - <sup>56</sup> M. Pustilnik and L. I. Glazman and W. Hofstetter, Phys. Rev. B **68**, 161303 (2003).
  - <sup>57</sup> M. Eto and Y. V. Nazarov, Phys. Rev. Lett. **85**, 1306 (2000).
  - <sup>58</sup> T. Kuzmenko, K. Kikoin and Y. Avishai, Phys. Rev. B **69**, 195109 (2004).
  - <sup>59</sup> W. Izumida, O. Sakai and S. Tarucha, Phys. Rev. Lett. **87**, 216803 (2001).
  - <sup>60</sup> J. A. White, Phys. Rev. B **45**, 1100 (1992).